Structure

Article

CHCHD4 binding affects the active site of apoptosis inducing factor (AIF): Structural determinants for allosteric regulation

Graphical abstract

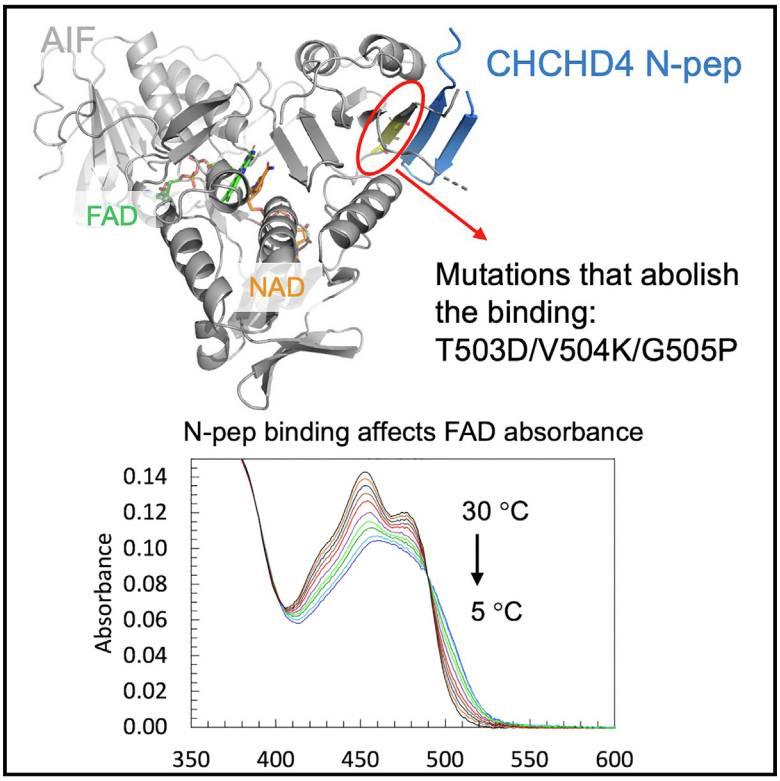

Highlights

- CHCHD4 binds to the C-ter domain of AIF and forms an intermolecular beta sheet
- Binding of CHCHD4 causes a structural transition in the active site of AIF
- AIF T503D/V504K/G505P triple mutant abolishes CHCHD4 binding

Authors

Elisa Fagnani, Paolo Cocomazzi, Sara Pellegrino, ..., Alessandro Aliverti, Eloise Mastrangelo, Mario Milani

Correspondence

alessandro.aliverti@unimi.it (A.A.), eloise.mastrangelo@cnr.it (E.M.), mario.milani@cnr.it (M.M.)

In brief

Fagnani et al. report the structure of the AIF protein in complex with a portion of the partner protein CHCHD4. The structural analysis together with additional experimental evidence shows that binding of CHCHD4 affects the active site of AIF. The structural plasticity of the AIF C-loop is important for binding.

Fagnani et al., 2024, Structure *32*, 1–13
May 2, 2024
https://doi.org/10.1016/j.str.2024.02.008

CellPress

Structure

CellPress
OPEN ACCESS

Article

CHCHD4 binding affects the active site of apoptosis inducing factor (AIF): Structural determinants for allosteric regulation

Elisa Fagnani,[1,2,7] Paolo Cocomazzi,[1,2,7] Sara Pellegrino,[3] Gabriella Tedeschi,[4,5] Francesca Grassi Scalvini,[4] Federica Cossu,[1,2] Stefano Da Vela,[6] Alessandro Aliverti,[2,*] Eloise Mastrangelo,[1,2,*] and Mario Milani[1,2,8,*]

[1]Biophysics Institute, CNR-IBF, Via Corti 12, 20133 Milan, Italy
[2]Department of Bioscience, Università degli Studi di Milano, Via Celoria 26, 20133 Milan, Italy
[3]Department of Pharmaceutical Sciences, Università degli Studi di Milano, Via Golgi 19, 20133 Milan, Italy
[4]Department of Veterinary Medicine and Animal Science (DIVAS), Università degli Studi di Milano, Via dell'Università 6, 26900 Lodi, Italy
[5]Cimaina, Università degli Studi di Milano, Milan, Italy
[6]Hochschule Bremerhaven, Karlstadt 8, 27568 Bremerhaven, Germany
[7]These authors contributed equally
[8]Lead contact
*Correspondence: alessandro.aliverti@unimi.it (A.A.), eloise.mastrangelo@cnr.it (E.M.), mario.milani@cnr.it (M.M.)
https://doi.org/10.1016/j.str.2024.02.008

SUMMARY

Apoptosis-inducing factor (AIF), which is confined to mitochondria of normal healthy cells, is the first identified caspase-independent cell death effector. Moreover, AIF is required for the optimal functioning of the respiratory chain machinery. Recent findings have revealed that AIF fulfills its pro-survival function by interacting with CHCHD4, a soluble mitochondrial protein which promotes the entrance and the oxidative folding of different proteins in the inner membrane space. Here, we report the crystal structure of the ternary complex involving the N-terminal 27-mer peptide of CHCHD4, NAD^+, and AIF harboring its FAD (flavin adenine dinucleotide) prosthetic group in oxidized form. Combining this information with biophysical and biochemical data on the CHCHD4/AIF complex, we provide a detailed structural description of the interaction between the two proteins, validated by both chemical cross-linking mass spectrometry analysis and site-directed mutagenesis.

INTRODUCTION

The apoptosis inducing factor (AIF)[1,2] is a highly conserved mitochondrial flavoprotein[3] that belongs to the glutathione reductase (GR) structural superfamily[4,5], and, in humans, is encoded by the *AIFM1* gene, located on the X chromosome.[1]

AIF is addressed to the mitochondria by an N-terminal localization sequence (proteolytically removed during or after translocation)[1] and once in the intermembrane space (IMS), it acquires the FAD (flavin adenine dinucleotide) cofactor and tethers to the inner membrane through its N-terminal segment. The protein is constituted of three domains: the first two, i.e., the FAD-binding domain (amino acids (aa.) 129–170, 203–262, and 400–479) and the NAD(P)H-binding domain (aa. 171–202 and 263–399), display the Rossmann fold topology, whereas the C-terminal domain (aa. 478–610) is composed of a β-sheet (with five antiparallel β-strands) and two α-helices.[6,7]

In addition to its well known but still under study pro-apoptotic function,[8,9] which is also related to its recently reported intrinsic nuclease activity,[10] AIF has an important role for efficient oxidative phosphorylation (OXPHOS)[11,12] related to the formation of a highly stable $FADH^-$-NAD^+ charge-transfer (CT) complex.[13] CT complex formation triggers conformational rearrangements, including the release of the C-loop (residues 509–561 of the C-terminal domain) from the protein core,[14] resulting in AIF dimerization,[15,16] suggesting a possible role of the protein as a redox sensor in the mitochondrial intermembrane space.[17] Such hypothesis is supported by the discovery of the interaction between AIF and CHCHD4 (the ortholog of yeast protein Mia40), a crucial component of the redox-regulated MIA machinery, responsible for the import and assembly of different proteins,[18,19] including substrates implicated in the biogenesis of respiratory chain complexes.[20–22]

AIF depletion is therefore associated with respiratory chain defects coupled with post-translational downregulation of respiratory chain complexes I, III, and VI.[23–26] To date more than 20 missense mutations in the *AIFM1* gene were found as the cause of several diseases, nine of which have been reported as mitochondrial disorders, displaying neurodegeneration as a common symptom.[27–32]

In this study, we investigate the interaction of AIF both with CHCHD4 and with a peptide corresponding to its N-terminal 27-residues (N-pep), known to be necessary and sufficient for the interaction.[33] Using a combination of biophysical techniques

Please cite this article in press as: Fagnani et al., CHCHD4 binding affects the active site of apoptosis inducing factor (AIF): Structural determinants for allosteric regulation, Structure (2024), https://doi.org/10.1016/j.str.2024.02.008

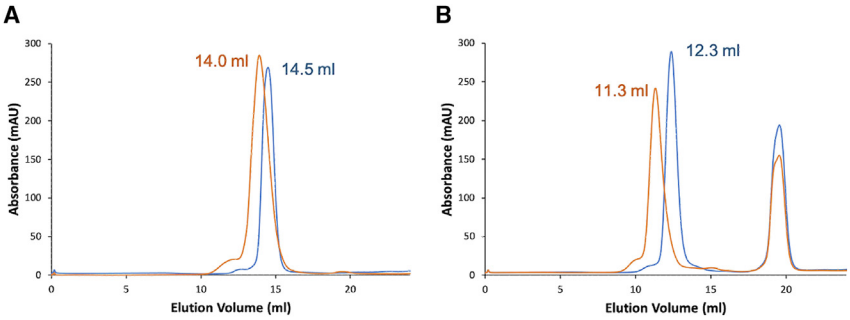

Figure 1. Effect of CHCHD4 on the retention time of AIF in gel filtration

Analyses were carried out at 9°C on samples pre-incubated for 1 h either in the absence or in the presence of NADH; elution volumes are reported on the corresponding peak.

(A) Superposed chromatograms of AIF (light blue) and of AIF/CHCHD4 mixture (orange), preincubated in the presence of NADH. The peaks at ~19.5 mL correspond to NADH.

(B) Superposed chromatograms of AIF (light blue) and of an AIF/CHCHD4 mixture (orange), pre-incubated in the absence of NADH. The decrease of retention times induced by NADH is due to redox-dependent AIF dimerization.

and structural biology analysis, our results show that the N-terminus of CHCHD4 acquires a beta hairpin structure as it binds to the C-terminal domain of AIF with the formation of an intermolecular beta sheet linking the two proteins. Our structural model is validated by cross-linking/mass spectrometry analysis and by substitution of three adjacent amino acids of AIF that abolishes the interaction of the two proteins.

RESULTS

SEC analysis of the complex between AIF and CHCHD4

It has been reported that AIF is able to form a very tight complex with CHCHD4,[33,34] provided that its FAD prosthetic group is kept in reduced form by the presence of NADH. Indeed, as shown in Figure 1A, we found that the complex between reduced AIF (from amino acid Gly102; Uniprot: Q9Z0X1) and CHCHD4 can be isolated by gel filtration, as indicated by the ~1 mL shift in retention time. Notably, this also excludes any significant FAD reoxidation within the analysis time, where the NADH excess is removed by chromatography, indicating an extremely slow oxidase activity of AIF under the experimental conditions. Quite surprisingly, we observed an analogous shift (~0.5 mL) also in the absence of NADH (Figure 1B), indicating that even oxidized AIF is able to establish a stable interaction with CHCHD4 during the chromatography run time. Notably, the complex involving oxidized AIF was not detectable when the SEC temperature was raised from 9°C to 25°C, indicating a strong temperature dependence of the interaction.

Perturbations of the AIF-bound FAD cofactor induced by the interaction with CHCHD4, N-pep, and NAD^+

As shown in Figures 2A and 2B, the addition of small excess of CHCHD4 (25.4 μM) to AIF (12.1 μM) at 25°C elicits a significant spectral change in the FAD prosthetic group, clearly indicating a structural rearrangement in the active site of the protein. Interestingly, while the addition of a large excess of NAD^+ (~6 mM) does not result in any change in FAD absorbance, i.e., no close binding of the two molecules, in the presence of CHCHD4 it induces a significant red-shift (Figure 2B, blue line), suggesting the formation of a stacking interaction between NAD^+ and the isoalloxazine ring of FAD.[35] Interestingly, the same stacking interaction (Figures 2C and 2D) is also promoted by the N-pep, indicating that the binding of the N-terminal portion of CHCHD4 determines a significant structural transition in the active site of AIF, making it accessible to the NAD^+ dinucleotide. Moreover, we found that the stacking interaction was promoted by lowering the temperature (Figures 2C and 2D). Since NAD^+ alone failed to induce any spectral change, we can infer that the temperature-sensitive step of the process is the binding of the N-pep, which is favored at low temperature as already observed for the binding of CHCHD4 to oxidized AIF (SEC experiments).

AIF/CHCHD4 cross-linking and mass spectrometry analysis

The binding between AIF and CHCHD4 was analyzed by cross-linking experiments incubating 27 μM of oxidized AIF with 40 μM of CHCHD4 in the presence of an excess of BS3 (2 mM). SDS gel electrophoresis showed the fast formation (after 5 min of reaction time) of covalent adducts with molecular weight compatible with that of the heterodimer AIF:CHCHD4 (~75 kDa; Figure 3A). Mass spectrometry analysis of the newly formed complexes (excised from the gel bands) showed the presence of a covalent bond between Lys517 of AIF—belonging to the C-loop (aa. 509–561)—and the N-terminal amine of CHCHD4, demonstrating that the interaction between the two proteins involves the C-ter domain of AIF and the N-ter segment of CHCHD4 (Figure 3A). An additional cross-link between Lys133 (CHCHD4) and Lys177 (AIF) was identified in the broadband with molecular weight between 130 and 150 kDa, corresponding to the formation of heterotrimers and heterotetramers of the complex (Figure 3A; Table S1).

AlphaFold model of AIF-CHCHD4

A model of the interaction between murine AIF and CHCHD4 was produced by using AlphaFold (see Figure S1 for quality scores). As expected, the model is highly similar to that already described by Pei et al.,[34] where the complex is stabilized by the interaction between the C-ter domain of AIF and the N-terminal portion of CHCHD4 (i.e., the N-pep).[33]

In the AlphaFold model, the C-loop is in closed conformation, as observed in the structures of the monomeric/oxidized protein (PDB: 4BV6 and 3GD3) and the two residues covalently bonded in our cross-linking/mass spectrometry experiments—Lys517 and the terminal amino group of CHCHD4—are at ~28 Å distance (Figure 3B). Therefore, a different conformation of the C-loop is necessary to allow a mutual distance compatible with the length of the BS3 linker (~13 Å). We can speculate

Please cite this article in press as: Fagnani et al., CHCHD4 binding affects the active site of apoptosis inducing factor (AIF): Structural determinants for allosteric regulation, Structure (2024), https://doi.org/10.1016/j.str.2024.02.008

CellPress
OPEN ACCESS

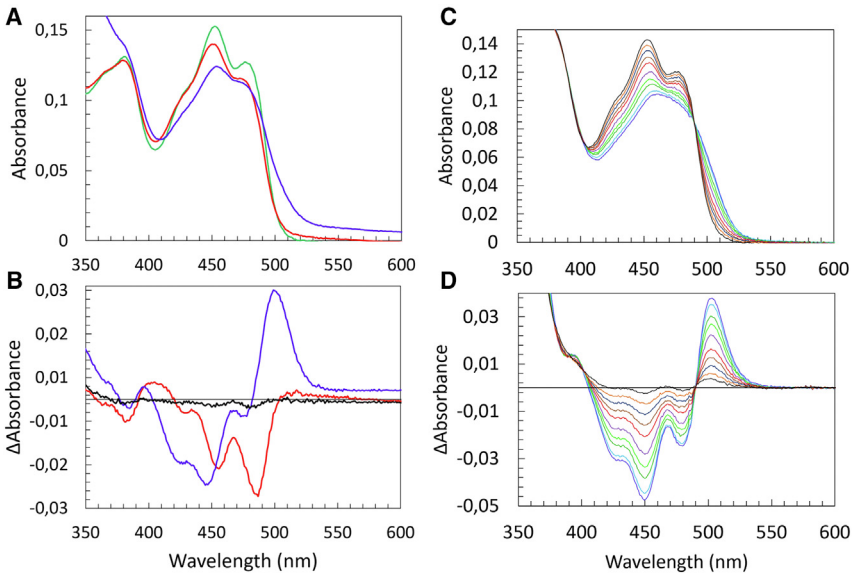

Figure 2. Changes induced in the absorbance spectrum of AIF by the binding of different ligands

(A and B) AIF, CHCHD4, and NAD^+ are 12.1 μM, 25.4 μM, and 3.75 mM, respectively, in 50 mM Tris-HCl, pH 8.0 (25°C). CHCHD4 does not significantly contribute to the absorbance of the samples within the explored wavelength range. (A) absorbance spectra of: 1. a mixture of AIF and CHCHD4 (red curve); 2. the sum of the two isolated proteins (green); 3. a mixture of AIF, CHCHD4 and NAD^+ (blue). (B) difference spectra between AIF and: 1. AIF/CHCHD4 (red); 2. AIF/NAD^+ (black) and 3. AIF/CHCHD4/NAD^+ (blue).

(C) Spectra and (D) difference spectra (calculated by subtracting the spectra of AIF and NAD^+ at the same concentrations) of the mixture of AIF, N-pep, and NAD^+ (12.1 μM, 139 μM, and 6.24 mM, respectively, in 50 mM Tris-HCl, pH 8.0) at 30°C (black), 25.5°C (orange), 23.5°C (dark blue), 21.5°C (brown), 20°C (red), 18°C (purple), 16°C (light green), 14°C (green) 10°C (light blue), and 5°C (blue).

that such different conformation of the C-loop in the oxidized AIF is induced by the binding of CHCHD4.

Crystal structure of oxidized AIF/NAD^+/N-pep complex

As expected, considering that the affinity of oxidized AIF (in the presence of NAD^+) for CHCHD4 or N-pep is enhanced at low temperature, the crystals of oxidized AIF/N-pep were obtained at 4°C in the presence of NAD^+.

The diffraction data were collected at ESRF beamline ID30A-1 and processed using the autoPROC package[36] (Table 1). The structure of the complex was solved by the molecular replacement method using as model the dimeric assembly of NAD-bound murine AIF (PDB: 3GD4[37]). After the placement of four AIF molecules in the crystal asymmetric unit (a.u.), the first refinement cycles showed a residual electron density near the AIF β-strand 503–507 (Figure S3A) that was modeled with a portion of the N-pep.

Several cycles of manual rebuilding (program Coot)[38] and refinement using *Refmac5*[39,40], *Phenix*[41], and *Buster*[42] produced the refined model. The overall structure of AIF is more similar to that of reduced than oxidized form of the protein, considering both the r.m.s.d. (0.91 vs. 1.18 Å, respectively (on 434 amino acids)) and the conformation of the 191–201 β-hairpin. The quality of electron density of the four AIF/N-pep complexes in the crystal a.u. is not homogeneous (as also indicated by the average values of B factors reported in Table 1), with the higher quality corresponding to the complex between AIF chain A and N-pep chain M (A/M complex) and the lower to the J/P complex. The 4 chains of AIF in the a.u. started from Ile125/Pro128 and terminated at Leu611/Glu613 (lacking ~22 residues at the N- and C-terminal ends of the construct). Moreover, most of the C-loop of all the 4 chains was not modeled (missing residues: chain A: 512–549, D: 508–556, G: 512–556, and J: 508–556) and the N-pep was modeled from Met1/Thr3 to His20/Ser25, therefore lacking the last seven or two C-terminal amino acids (Figure 4A).

In previous NMR experiments, the N-ter domain of CHCHD4 was shown to be unstructured.[20] In our crystal structure, the N-pep forms a β-hairpin that binds to the C-terminal domain of AIF as predicted by the AlphaFold model.[34] The β-hairpin is constituted of beta strands β1 (Cys4-Glu7) and β2 (Asp10-Phe14) with the β-turn (Gly8-Lys9) stabilized by the intramolecular salt bridge between Lys9 and Asp10 (the latter in H-bond with the side chain of AIF Thr503; Figure 4B). The protein-protein interaction is based on the β2 strand of CHCHD4 that forms an intermolecular β-sheet with the β-strand Thr503-Phe507 of AIF (Figure 4B). The binding is further stabilized by two hydrophobic patches: in the first, N-pep Ile12 and Phe14 are hosted in the hydrophobic cleft made by Tyr346, Phe507, and Tyr559, and, on the opposite side of the β-strand, N-pep Ile13 is in close contact with Val504 and Val506. Both the N-terminal portion of β1 and the C-terminal end of the N-pep (from Lys17 to His20) are more flexible, as shown from the superposition of the 4 copies of the complex in the crystal a.u. (Figure 4B).

As already mentioned, unlike what was observed in the crystal structures of oxidized AIF, it was not possible to model most of the C-loop, probably due to its conformational freedom in the crystal. Such evidence suggests that the binding of the N-pep (or of CHCHD4) induces a structural rearrangement of the C-loop compatible with the formation of the covalent bond between Lys517 and CHCHD4 N-terminus. Finally, as expected from the spectroscopic analysis, in the active site of AIF the NAD^+ establishes a stacking interaction with FAD (Figure 4A) similarly to what was observed in the structure of the reduced protein (PDB: 3GD4).

Small-angle X-ray scattering (SAXS)

SEC-SAXS data were collected on both AIF oxidized/reduced state, and on CHCHD4 alone or in presence of reduced AIF. The data were analyzed with *CHROMIXS*[43] and *PRIMUS* software (Table S3, ATSAS suite).[44]

CHCHD4. SEC-SAXS analysis of CHCHD4 (Mw 17.0 kDa) showed a single elution peak with a big gyration radius (Rg = 2.7 ± 0.3 nm), and with an estimated molecular weight corresponding to a monomeric assembly (Bayesian analysis Mw = 16.1 kDa). The program *dammin*[45] builts models with elongated

Please cite this article in press as: Fagnani et al., CHCHD4 binding affects the active site of apoptosis inducing factor (AIF): Structural determinants for allosteric regulation, Structure (2024), https://doi.org/10.1016/j.str.2024.02.008

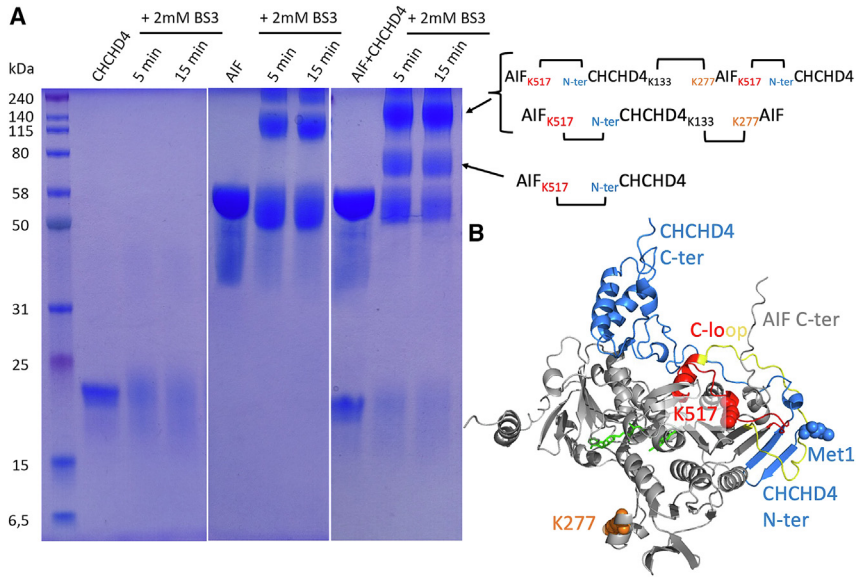

Figure 3. AIF/CHCHD4 interaction analysis

(A) Cross-linking of AIF/CHCHD4 mixture as analyzed by SDS-PAGE.

(B) Cartoon representation of the AlphaFold model of the complex between a monomer of AIF (gray) and a monomer of CHCHD4 (blue); the C-loop is colored in red (N-terminal half: aa. 508–534) and in yellow (C-terminal half: aa. 535–562); the amino acids observed in covalent bond, i.e., Lys517 and the N-terminus of CHCHD4, are represented with spheres in red and blue, respectively; Lys277, the additional amino acid observed in covalent bond, is represented with orange spheres; CHCHD4 K133, being located in the disordered C-terminal end of the protein (starting from Lys116), is not shown; the FAD is in green sticks. Figures were prepared using PyMOL.

structures (gnome Dmax = 7.95 nm)[46] composed of 4–5 small independent domains (Figure 5B), qualitatively not dissimilar from the AlphaFold model (https://alphafold.ebi.ac.uk/Q8VEA4).

AIF oxidized/monomeric state. The monomeric/oxidized AIF protein in solution displays a gyration radius (Rg = 2.65 ± 0.05 nm) consistent with that observed for the human protein (Rg = 2.61 nm; AIF121).[14] The crystallographic monomeric model of the protein with the addition of the missing N-ter residues (produced by AlphaFold) displayed a lower gyration radius (Rg = 2.53 nm; calculated using program *crysol*).[47] Interestingly, a similar slight difference between experimental and model gyration radii values was also observed for the human protein (model/experimental Rg = 2.53/2.61 nm, respectively).[14]

AIF reduced/dimeric state. The SAXS-SEC analysis of the reduced AIF displays a gyration radius of 3.69 ± 0.05 nm, with an estimated Bayesian Mw of 113.7 kDa (Figure 5A), in agreement with the dimeric assembly (114.2 kDa; Dmax = 12.2 nm). The structure of the dimeric assembly, obtained superposing the AlphaFold model of the monomer on the crystallographic dimer of the oxidized structure (PDB: 3GD3), with the closed conformation of the C-loop, is in fair agreement with SEC-SAXS data (*crysol* Chi^2 = 2.37). However, after the generation of 650 random non-symmetric conformations of the C-loop (from Ala508 to Gly562; program *Loop sampler*[48] (https://moma.laas.fr/)) in the context of the dimeric assembly, the vast majority of the new structures (96%) were in better agreement with the experimental data (best *crysol* Chi^2 = 1.47; Figure S4), suggesting that the C-loop likely adopts an open conformation in the reduced/dimeric state as already described by Brosey et al.[14]

AIF reduced dimeric state in complex with CHCHD4. The SEC of the reduced AIF in the presence of CHCHD4 showed the presence of a single elution peak with a gyration radius of 4.3 ± 0.1 nm, with an estimated Bayesian Mw of 146.8 kDa (Figure 5C), in agreement with the expected heterotetrametric assembly (148.2 kDa). The AlphaFold model of the tetrameric complex between the AIF dimer and two CHCHD4 molecules is not in good agreement with the SEC-SAXS data (*crysol* Chi^2 = 32.9) and the discrepancy can only be partially reduced by modeling 650 random non-symmetric conformations of the C-loop (best *crysol* Chi^2 = 3.30), suggesting that probably the C-terminal domain of CHCHD4 is not correctly modeled in the context of the dimeric assembly. Anyhow the Kratky plot shows that the AIF-CHCHD4 complex is mostly folded, suggesting that also the N-terminal domain of CHCHD4 is likely interacting with AIF (Figure S5).

The triple mutant T503D/V504K/G505P abolishes AIF binding to CHCHD4

The analysis of the crystal structure of AIF/N-pep interaction allowed the design of an AIF variant predicted to hinder the formation of the complex. In detail, the mutations Thr503Asp and Val504Lys were thought to induce electrostatic repulsion, being in close contact with the residues Asp10 and Arg11 of CHCHD4, respectively, and the mutation Gly505Pro was predicted to weaken the intermolecular β sheet by eliminating the H-bond with Arg11 carbonyl.

The triple mutant T503D/V504K/G505P (mutAIF) displayed a significantly lower expression yield with respect to the wild-type (WT) protein, suggesting that the mutations partially impaired the correct folding of the protein. However, no difference with WT AIF was observed during the purification of the protein, indicating that mutAIF was stable after its folding. Moreover, the FAD absorbance spectrum is identical to that of the WT form (not shown) demonstrating that the active site of the protein is unaffected by the mutations. Indeed, the three residue replacements have only a limited effect on the folding stability of AIF in both its oxidized and CT complex states, decreasing the melting temperature (T_m) by just 3.5°C and 5.5°C, respectively (Table 2).

Interestingly, while the addition of CHCHD4 determines a decrease in T_m for WT AIF, it has no effect on mutAIF, suggesting the absence of binding (Figure S6). We have already shown that the NADH-induced CT complex formation destabilizes AIF.[15] Surprisingly, we show that NAD^+ can produce a similar effect, demonstrating that, even without inducing any spectral change in the FAD cofactor (see previous sections), the oxidized dinucleotide is able to bind to AIF. Again, while the addition of CHCHD4 greatly enhances the destabilizing effect of NAD^+ for the WT

Please cite this article in press as: Fagnani et al., CHCHD4 binding affects the active site of apoptosis inducing factor (AIF): Structural determinants for allosteric regulation, Structure (2024), https://doi.org/10.1016/j.str.2024.02.008

CellPress
OPEN ACCESS

Table 1. X-ray data-collection and refinement statistics

Data collection	
Beamline & wavelength (Å)	ESRF ID30A-1 0.96546
Space group	$P2_12_12_1$
Unit-cell parameters (Å)	a = 110.1; b = 115.6; c = 192.7
heterodimers in a.u.	4
Resolution (Å)	99.1–3.206 (3.483-3.206)
Unique reflections	24,919 (1,247)
Completeness (spherical) (%)	60.7 (14.0)
Completeness (ellipsoidal) (%)	93.6 (64.6)
Multiplicity	13.2 (13.6)
Rmeas[a] (%)	31.5 (195.1)
CC(1/2) (%)	99.6 (65.6)
Average I/σ (I)	7.6 (1.6)
Final model	
R factor[b]/Rfree[c] (%)	23.3/28.4
r.m.s. bonds (Å)	0.006
r.m.s. angles (°)	1.20
Residues in most favored regions (%)	92.8
Residues in additionally allowed regions (%)	6.6
<B> AIF [Å^2][d]	A: 55.1; D: 68.4; G:77.6; J:110.9
<B> N-pep [Å^2][d]	M: 71.8; N: 78.3; O:116.4; P:89.1
<B> Waters [Å^2][d]	61.8
PDB	8QNS

Values in parentheses are for the highest resolution shell: 3.483-3.206
[a]$R_{meas} = (\Sigma (n/(n-1) \Sigma |I - (I)|)/\Sigma I \times 100$, where I is the intensity of a reflection and (I) is its average intensity.
[b]$R_{factor} = \Sigma |F_o - F_c|/\Sigma |F_o| \times 100$.
[c]R_{free} is calculated on 5% randomly selected reflections, for cross-validation.
[d]Chains of the AIF/N-pep complex: A/M, D/O, G/N, J/P.

protein (ΔTm = -10°C), it has a negligible effect on mutAIF, suggesting again that the triple mutant is unable to bind CHCHD4.

The binding between AIF and CHCHD4 was further analyzed by microscale thermophoresis (MST), exploiting either the perturbation of thermal diffusion or the change in the fluorescence emission of labeled AIF. Oxidized AIF was able to bind CHCHD4 with medium affinity (K_d = 13 ± 2 μM), and upon FAD reduction by NADH the affinity increased by ∼150-fold (K_d = 85 ± 15 nM), value comparable to that already reported by Romero-Tamayo et al.[49] (Figure S7). Notably, AIF binds to N-pep with K_d values indistinguishable from those of the full-length protein (K_d = 15 ± 5 μM and 76 ± 2 nM, for the oxidized and reduced form, respectively), confirming that the first 27 residues of CHCHD4 are responsible for the entire free energy of binding. As expected, both MST and analytical gel filtration do not show any binding between mutAIF and CHCHD4 (Figure S8). Finally, no SDS-PAGE band attributable to mutAIF/CHCHD4 covalent adduct was detected after treatment with the BS3 cross-linker (not shown).

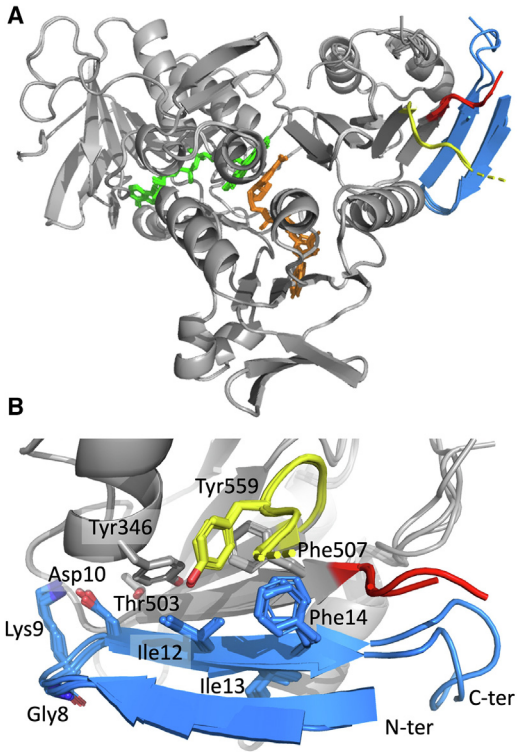

Figure 4. Crystal structure of the complex between AIF and N-pep
(A) Superposition of the four AIF/N-pep structures in the asymmetric unit of the crystal in gray/blue cartoons, respectively. The visible portions of the C-loop are colored in red (N-ter) and yellow (C-ter); FAD and NAD^+ are represented as green and orange sticks, respectively.
(B) Detail of the interaction between AIF and N-pep (gray/blue cartoons) with selected residues represented as sticks and labeled.

DISCUSSION

The formation of AIF-CHCHD4 heterotetrametric complex is a key element for the mitochondria import of specific proteins since monomeric CHCHD4 does not interact efficiently nor mediate the import of specific substrates.[50] AIF mutations that impair the interaction with CHCHD4 lead to different diseases including auditory neuropathy disorder.[51]

In this work, the interaction between the two proteins is studied by different techniques including SEC, thermophoresis, and thermal denaturation, demonstrating that CHCHD4 can bind AIF either in its oxidized or reduced form. However, the binding affinity changes depending on the oxidation state, being the K_d for the dimeric/reduced AIF (CT complex) two orders of magnitude lower than that for the monomeric/oxidized protein. Such evidence suggests that CHCHD4 binding can be affected by both AIF quaternary assembly (dimeric in CT complex) and/or by the conformation of the FAD binding site. Moreover, we show that the inverse influence is also present: CHCHD4 binding affects the structure of the AIF active site, allowing the stacking interaction between NAD^+ and oxidized FAD.

Although the N-terminus of CHCHD4 is known to be disordered in solution,[20] our crystal structure shows that the first 27 residues of the protein fold by interacting with AIF, forming a

Please cite this article in press as: Fagnani et al., CHCHD4 binding affects the active site of apoptosis inducing factor (AIF): Structural determinants for allosteric regulation, Structure (2024), https://doi.org/10.1016/j.str.2024.02.008

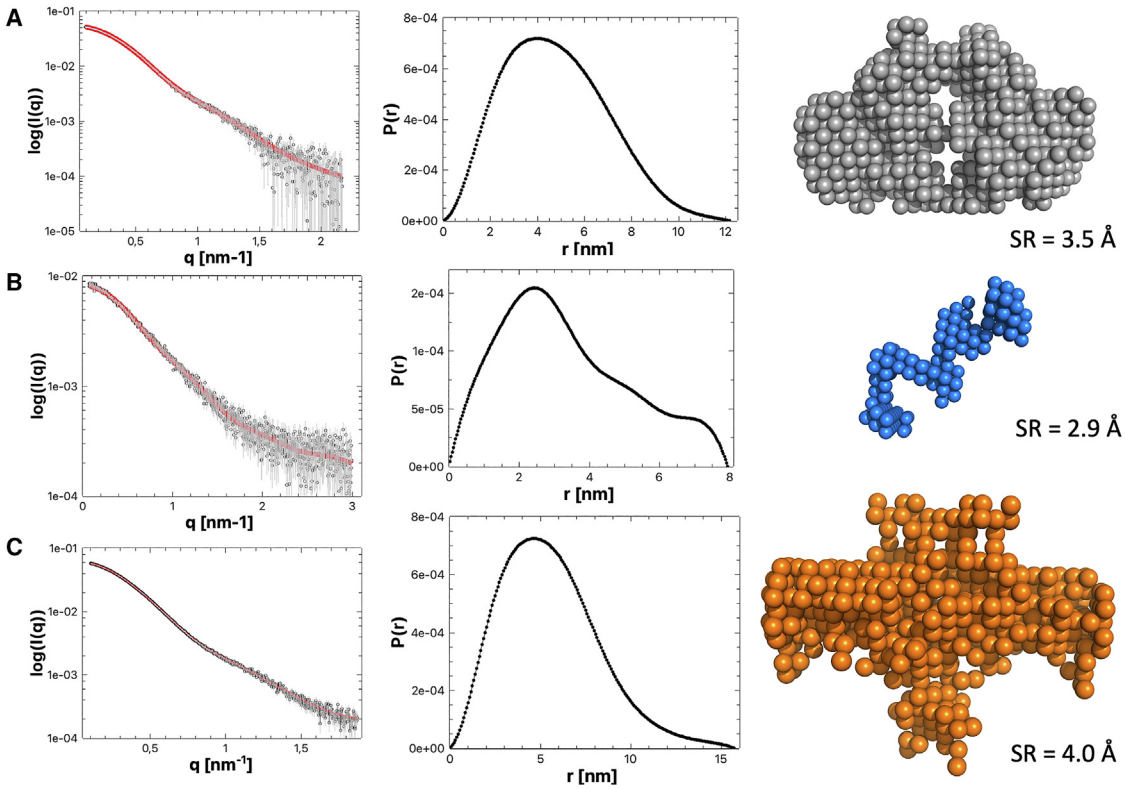

Figure 5. SEC-SAXS data analysis

Left graphs: SAXS data fitted by the *gnom* program (red line); central graphs: pair distance distribution, P(r); right figures: best *dammin* model (with different sphere radius (SR)) for: (A) reduced AIF, (B) CHCHD4, and (C) reduced AIF with CHCHD4.

β-hairpin. Together with cross-linking experiments, the crystallographic analysis shows that the binding site of CHCHD4 is located at the C-terminal domain of AIF. Accordingly, targeted replacements of the selected amino acids 503–505 result in a protein incapable of binding CHCHD4, as shown by MST, analytical gel filtration and BS3 cross-linking experiments.

The considerable distance between the AIF active site and the CHCHD4 binding site requires the presence of some long-range allosteric mechanism to enable their mutual influence.

In previous crystallographic analysis, the AIF C-loop was observed in two different conformations in the oxidized (monomeric) or the reduced (dimeric) forms. In the former, it is ordered (with only ∼15 residues not modeled) with residues Ile527 and Ser529 (Ile528 and Ser530 in the human protein, PDB: 4BV6) close to the FAD cofactor. In the reduced/dimeric form, the C-loop is mostly disordered [with about only twenty residues modeled; PDB: 4BUR (human) and 3GD4 (mouse)], solvent exposed and partially structured as an additional parallel (residues 539–543 in the mouse protein) or antiparallel (residues 511–515, in the human protein) β-strand, interacting with C-terminal strand 503–508.

In our crystal structure (oxidized FAD), we observe an analogous beta-beta interaction between the AIF C-terminal β-strand 503–508 and the β-strand 10–14 of CHCHD4 (Figure 4), with the C-loop presumably assuming a solvent-exposed open conformation to account for the formation of the covalent link between Lys517 and the N-terminus of CHCHD4. Therefore, the C-loop conformational plasticity provides a possible mechanism for the mutual influence between the AIF active site and the CHCHD4 binding site.

Previous work on human AIF already identified an allosteric pathway propagating from the active site of the CT complex: the binding of NAD induces the repositioning of Phe482 and Phe310 (in stacking interaction with the nicotinamide ring) that

Table 2. Melting temperatures of wild type AIF and mutAIF in the presence of different ligands

	Ligand					
	None	NADH[a]	CHCHD4	NADH/CHCHD4[a]	NAD^+	NAD^+/CHCHD4
AIF	T_m (°C)					
WT	73.0 ± 0.5	57.0 ± 0.5	63.0 ± 0.8	58.0 ± 0.5	61.0 ± 0.5	51.0 ± 0.9
mut	69.5 ± 0.5	51.5 ± 0.5	68.5 ± 0.5	51.5 ± 0.5	58.0 ± 0.5	62.5 ± 0.5

[a]Incubation in the presence of NADH leads to FAD reduction and generation of the CT complex.

is transmitted through His454 to Ser480 and to the whole hydrophobic patch Phe482-Phe310-Tyr491. The resulting displacement of β-strand 481–487 causes the release of the "Cβ-clasp" (i.e., the portion of the C-loop interacting with β-hairpin 487-490) and thus the opening of the C-loop.[14]

Following the previous findings, we can speculate that the signal from the AIF active site to CHCHD4 binding site starts from the formation of the stacking interaction between NAD^+ and $FADH^-$ in the CT complex, and is transmitted through the opening of the C-loop — observed in different crystal structures and in our SAXS experiments — to the CHCHD4 binding site, as shown by the enhanced affinity of the reduced AIF for the partner protein. Analogously, the opposite signal from CHCHD4 binding site to the AIF active site would start from the binding of CHCHD4 that induces the opening of the C-loop — as suggested by the decrease in T_m of the complex, by our crystal structure and by the cross-linking experiments — allowing the formation of the NAD^+/FAD stacking interaction (as shown by the spectroscopic analysis). To further support this picture, it is worth noticing that binding of CHCHD4 or NADH/NAD^+ induces a reduction in the thermal stability of AIF, which can be explained by the opening of the C-loop.

A further element in the proposed mechanism arises from the presumed location of the ~15 not modeled residues in oxidized AIF C-loop (closed conformation of the C-loop): these residues are probably located in front of the β-strand 503–508 hindering the formation of new β-β interactions (as suggested by the lower affinity of oxidized AIF for CHCHD4). The C-loop opening is thus necessary to release such protection, allowing the β-strand 503–508 to participate in both transient (with different portions of the C-loop itself) or stable (with CHCHD4) new interactions.

To summarize, in this paper, we describe the binding mode of the CHCHD4 N-terminal domain to the C-terminal domain of AIF and demonstrate how such interaction allosterically affects the FAD binding site of the protein likely through C-loop repositioning.

STAR★METHODS

Detailed methods are provided in the online version of this paper and include the following:

SUPPLEMENTAL INFORMATION

Supplemental information can be found online at https://doi.org/10.1016/j.str.2024.02.008.

ACKNOWLEDGMENTS

We acknowledge the European Union - Next Generation EU - PNRR, MUR code IR0000011, CUP B51E22000150006, project "EBRAINS-Italy - European Brain ReseArch INfrastructureS Italy" for financial support. We acknowledge the European Synchrotron Radiation Facility (ESRF) for provision of synchrotron radiation facilities, and particularly the people working at the beamline ID30A1. We acknowledge the Deutsches Elektronen-Synchrotron (DESY) of Hamburg and the people working at beamline P12 for helping us during SAXS data collection. EMBO Short-Term Fellowship n° 8159 with a project entitled "Interaction between the Apoptosis Inducing Factor (AIF) and CHCHD4: a possible connection to mitochondriopathies onset" (2019). The work was supported in part by grant "Linea 2, 2021, from Università degli Studi di Milano to A. A.

AUTHOR CONTRIBUTIONS

M.M. A.A., and E.M. supervised the project, designed research, wrote the paper. E.F. and P.C. protein expression and purification, biochemistry, X-ray crystallography, and SAXS experiment. S.P. synthesis of the CHCHD4 peptide. G.T. and F.G.S. mass spectrometry analysis. F.C. designed research. S.D.V. SAXS experiments. All authors contributed to the editing of the manuscript.

DECLARATION OF INTERESTS

The authors declare no competing interests.

Received: October 3, 2023
Revised: January 8, 2024
Accepted: February 13, 2024
Published: March 8, 2024

REFERENCES

1. Susin, S.A., Lorenzo, H.K., Zamzami, N., Marzo, I., Snow, B.E., Brothers, G.M., Mangion, J., Jacotot, E., Costantini, P., Loeffler, M., et al. (1999). Molecular characterization of mitochondrial apoptosis-inducing factor. Nature *397*, 441–446. https://doi.org/10.1038/17135.
2. Sevrioukova, I.F. (2011). Apoptosis-inducing factor: structure, function, and redox regulation. Antioxid. Redox Signal. *14*, 2545–2579. https://doi.org/10.1089/ARS.2010.3445.
3. Lorenzo, H.K., Susin, S.A., Penninger, J., and Kroemer, G. (1999). Apoptosis inducing factor (AIF): a phylogenetically old, caspase-independent effector of cell death. Cell Death Differ. *6*, 516–524. https://doi.org/10.1038/sj.cdd.4400527.
4. Dym, O., and Eisenberg, D. (2001). Sequence-structure analysis of FAD-containing proteins. Protein Sci. *10*, 1712–1728. https://doi.org/10.1110/PS.12801.
5. Aliverti, A., Pandini, V., Pennati, A., de Rosa, M., and Zanetti, G. (2008). Structural and functional diversity of ferredoxin-NADP(+) reductases. Arch. Biochem. Biophys. *474*, 283–291. https://doi.org/10.1016/J.ABB.2008.02.014.
6. Maté, M.J., Ortiz-Lombardía, M., Boitel, B., Haouz, A., Tello, D., Susin, S.A., Penninger, J., Kroemer, G., and Alzari, P.M. (2002). The crystal structure of the mouse apoptosis-inducing factor AIF. Nat. Struct. Biol. *9*, 442–446. https://doi.org/10.1038/NSB793.

7. Ye, H., Cande, C., Stephanou, N.C., Jiang, S., Gurbuxani, S., Larochette, N., Daugas, E., Garrido, C., Kroemer, G., and Wu, H. (2002). DNA binding is required for the apoptogenic action of apoptosis inducing factor. Nat. Struct. Biol. *9*, 680–684. https://doi.org/10.1038/nsb836.

8. Aredia, F., and Scovassi, A.I. (2014). Poly(ADP-ribose): a signaling molecule in different paradigms of cell death. Biochem. Pharmacol. *92*, 157–163. https://doi.org/10.1016/J.BCP.2014.06.021.

9. Susin, S.A., Daugas, E., Ravagnan, L., Samejima, K., Zamzami, N., Loeffler, M., Costantini, P., Ferri, K.F., Irinopoulou, T., Prévost, M.C., et al. (2000). Two distinct pathways leading to nuclear apoptosis. J. Exp. Med. *192*, 571–580. https://doi.org/10.1084/JEM.192.4.571.

10. Novo, N., Romero-Tamayo, S., Marcuello, C., Boneta, S., Blasco-Machin, I., Velázquez-Campoy, A., Villanueva, R., Moreno-Loshuertos, R., Lostao, A., Medina, M., and Ferreira, P. (2023). Beyond a platform protein for the degradosome assembly: The Apoptosis-Inducing Factor as an efficient nuclease involved in chromatinolysis. PNAS Nexus *2*, pgac312. https://doi.org/10.1093/PNASNEXUS/PGAC312.

11. Joza, N., Pospisilik, J.A., Hangen, E., Hanada, T., Modjtahedi, N., Penninger, J.M., and Kroemer, G. (2009). AIF: not just an apoptosis-inducing factor. Ann. N. Y. Acad. Sci. *1171*, 2–11. https://doi.org/10.1111/J.1749-6632.2009.04681.X.

12. Norberg, E., Orrenius, S., and Zhivotovsky, B. (2010). Mitochondrial regulation of cell death: processing of apoptosis-inducing factor (AIF). Biochem. Biophys. Res. Commun. *396*, 95–100. https://doi.org/10.1016/J.BBRC.2010.02.163.

13. Churbanova, I.Y., and Sevrioukova, I.F. (2008). Redox-dependent changes in molecular properties of mitochondrial apoptosis-inducing factor. J. Biol. Chem. *283*, 5622–5631. https://doi.org/10.1074/JBC.M709147200.

14. Brosey, C.A., Ho, C., Long, W.Z., Singh, S., Burnett, K., Hura, G.L., Nix, J.C., Bowman, G.R., Ellenberger, T., and Tainer, J.A. (2016). Defining NADH-Driven Allostery Regulating Apoptosis-Inducing Factor. Structure *24*, 2067–2079. https://doi.org/10.1016/J.STR.2016.09.012.

15. Sorrentino, L., Calogero, A.M., Pandini, V., Vanoni, M.A., Sevrioukova, I.F., and Aliverti, A. (2015). Key Role of the Adenylate Moiety and Integrity of the Adenylate-Binding Site for the NAD+/H Binding to Mitochondrial Apoptosis-Inducing Factor. Biochemistry *54*, 6996–7009. https://doi.org/10.1021/ACS.BIOCHEM.5B00898/ASSET/IMAGES/BI-2015-00898A_M006.GIF.

16. Sorrentino, L., Cossu, F., Milani, M., Aliverti, A., and Mastrangelo, E. (2017). Structural bases of the altered catalytic properties of a pathogenic variant of apoptosis inducing factor. Biochem. Biophys. Res. Commun. *490*, 1011–1017.

17. Novo, N., Ferreira, P., and Medina, M. (2021). The apoptosis-inducing factor family: Moonlighting proteins in the crosstalk between mitochondria and nuclei. IUBMB Life *73*, 568–581. https://doi.org/10.1002/IUB.2390.

18. Hofmann, S., Rothbauer, U., Mühlenbein, N., Baiker, K., Hell, K., and Bauer, M.F. (2005). Functional and Mutational Characterization of Human MIA40 Acting During Import into the Mitochondrial Intermembrane Space. J. Mol. Biol. *353*, 517–528. https://doi.org/10.1016/J.JMB.2005.08.064.

19. Petrungaro, C., Zimmermann, K.M., Küttner, V., Fischer, M., Dengjel, J., Bogeski, I., and Riemer, J. (2015). The Ca2+-Dependent Release of the Mia40-Induced MICU1-MICU2 Dimer from MCU Regulates Mitochondrial Ca2+ Uptake. Cell Metab. *22*, 721–733. https://doi.org/10.1016/J.CMET.2015.08.019.

20. Banci, L., Bertini, I., Cefaro, C., Ciofi-Baffoni, S., Gallo, A., Martinelli, M., Sideris, D.P., Katrakili, N., and Tokatlidis, K. (2009). MIA40 is an oxidoreductase that catalyzes oxidative protein folding in mitochondria. Nat. Struct. Mol. Biol. *16*, 198–206. https://doi.org/10.1038/nsmb.1553.

21. Dickson-Murray, E., Nedara, K., Modjtahedi, N., and Tokatlidis, K. (2021). The Mia40/CHCHD4 Oxidative Folding System: Redox Regulation and Signaling in the Mitochondrial Intermembrane Space. Antioxidants *10*, 592. https://doi.org/10.3390/ANTIOX10040592.

22. Chacinska, A., Pfannschmidt, S., Wiedemann, N., Kozjak, V., Sanjuán Szklarz, L.K., Schulze-Specking, A., Truscott, K.N., Guiard, B., Meisinger, C., and Pfanner, N. (2004). Essential role of Mia40 in import and assembly of mitochondrial intermembrane space proteins. EMBO J. *23*, 3735–3746. https://doi.org/10.1038/SJ.EMBOJ.7600389.

23. Vahsen, N., Candé, C., Brière, J.J., Bénit, P., Joza, N., Larochette, N., Mastroberardino, P.G., Pequignot, M.O., Casares, N., Lazar, V., et al. (2004). AIF deficiency compromises oxidative phosphorylation. EMBO J. *23*, 4679–4689. https://doi.org/10.1038/SJ.EMBOJ.7600461.

24. Brown, D., Yu, B.D., Joza, N., Benit, P., Meneses, J., Firpo, M., Rustin, P., Penninger, J.M., and Martin, G.R. (2006). Loss of Aif function causes cell death in the mouse embryo, but the temporal progression of patterning is normal. Proc. Natl. Acad. Sci. USA *103*, 9918–9923. https://doi.org/10.1073/PNAS.0603950103/SUPPL_FILE/03950FIG5.PDF.

25. Bénit, P., Goncalves, S., Dassa, E.P., Brière, J.J., and Rustin, P. (2008). The Variability of the Harlequin Mouse Phenotype Resembles that of Human Mitochondrial-Complex I-Deficiency Syndromes. PLoS One *3*, e3208. https://doi.org/10.1371/JOURNAL.PONE.0003208.

26. Pospisilik, J.A., Knauf, C., Joza, N., Benit, P., Orthofer, M., Cani, P.D., Ebersberger, I., Nakashima, T., Sarao, R., Neely, G., et al. (2007). Targeted deletion of AIF decreases mitochondrial oxidative phosphorylation and protects from obesity and diabetes. Cell *131*, 476–491. https://doi.org/10.1016/J.CELL.2007.08.047.

27. Heimer, G., Eyal, E., Zhu, X., Ruzzo, E.K., Marek-Yagel, D., Sagiv, D., Anikster, Y., Reznik-Wolf, H., Pras, E., Oz Levi, D., et al. (2018). Mutations in AIFM1 cause an X-linked childhood cerebellar ataxia partially responsive to riboflavin. Eur. J. Paediatr. Neurol. *22*, 93–101. https://doi.org/10.1016/J.EJPN.2017.09.004.

28. Sancho, P., Sánchez-Monteagudo, A., Collado, A., Marco-Marín, C., Domínguez-González, C., Camacho, A., Knecht, E., Espinós, C., and Lupo, V. (2017). A newly distal hereditary motor neuropathy caused by a rare AIFM1 mutation. Neurogenetics *18*, 245–250. https://doi.org/10.1007/S10048-017-0524-6/FIGURES/5.

29. Mierzewska, H., Rydzanicz, M., Biegański, T., Kosinska, J., Mierzewska-Schmidt, M., Ługowska, A., Pollak, A., Stawiński, P., Walczak, A., Kędra, A., et al. (2017). Spondyloepimetaphyseal dysplasia with neurodegeneration associated with AIFM1 mutation - a novel phenotype of the mitochondrial disease. Clin. Genet. *91*, 30–37. https://doi.org/10.1111/CGE.12792.

30. Bano, D., and Prehn, J.H.M. (2018). Apoptosis-Inducing Factor (AIF) in Physiology and Disease: The Tale of a Repented Natural Born Killer. EBioMedicine *30*, 29–37. https://doi.org/10.1016/J.EBIOM.2018.03.016.

31. Breuer, M.E., Koopman, W.J., Koene, S., Nooteboom, M., Rodenburg, R.J., Willems, P.H., and Smeitink, J.A.M. (2013). The role of mitochondrial OXPHOS dysfunction in the development of neurologic diseases. Neurobiol. Dis. *51*, 27–34. https://doi.org/10.1016/J.NBD.2012.03.007.

32. Wischhof, L., Scifo, E., Ehninger, D., and Bano, D. (2022). AIFM1 beyond cell death: An overview of this OXPHOS-inducing factor in mitochondrial diseases. EBioMedicine *83*, 104231. https://doi.org/10.1016/J.EBIOM.2022.104231.

33. Hangen, E., Féraud, O., Lachkar, S., Mou, H., Doti, N., Fimia, G.M., Lam, N.V., Zhu, C., Godin, I., Muller, K., et al. (2015). Interaction between AIF and CHCHD4 Regulates Respiratory Chain Biogenesis. Mol. Cell *58*, 1001–1014. https://doi.org/10.1016/J.MOLCEL.2015.04.020.

34. Pei, J., Zhang, J., and Cong, Q. (2022). Human mitochondrial protein complexes revealed by large-scale coevolution analysis and deep learning-based structure modeling. Bioinformatics *38*, 4301–4311. https://doi.org/10.1093/BIOINFORMATICS/BTAC527.

35. Deng, Z., Aliverti, A., Zanetti, G., Arakaki, A.K., Ottado, J., Orellano, E.G., Calcaterra, N.B., Ceccarelli, E.A., Carrillo, N., and Karplus, P.A. (1999). A productive NADP+ binding mode of ferredoxin–NADP+ reductase revealed by protein engineering and crystallographic studies. Nat. Struct. Biol. *6*, 847–853. https://doi.org/10.1038/12307.

36. Vonrhein, C., Flensburg, C., Keller, P., Sharff, A., Smart, O., Paciorek, W., Womack, T., and Bricogne, G. (2011). Data processing and analysis with the autoPROC toolbox *67*, 293–302. https://doi.org/10.1107/S0907444911007773.

37. Sevrioukova, I.F. (2009). Redox-Linked Conformational Dynamics in Apoptosis-Inducing Factor. J. Mol. Biol. *390*, 924–938. https://doi.org/10.1016/J.JMB.2009.05.013.

38. Emsley, P., Lohkamp, B., Scott, W.G., and Cowtan, K. (2010). Features and development of Coot. Acta Crystallogr. D Biol. Crystallogr. *66*, 486–501. https://doi.org/10.1107/S0907444910007493.

39. Winn, M.D., Ballard, C.C., Cowtan, K.D., Dodson, E.J., Emsley, P., Evans, P.R., Keegan, R.M., Krissinel, E.B., Leslie, A.G.W., McCoy, A., et al. (2011). Overview of the CCP4 suite and current developments. Acta Crystallogr. D Biol. Crystallogr. *67*, 235–242. https://doi.org/10.1107/S0907444910045749.

40. Murshudov, G.N., Skubák, P., Lebedev, A.A., Pannu, N.S., Steiner, R.A., Nicholls, R.A., Winn, M.D., Long, F., and Vagin, A.A. (2011). REFMAC5 for the refinement of macromolecular crystal structures. Acta Crystallogr. D Biol. Crystallogr. *67*, 355–367. https://doi.org/10.1107/S0907444911001314.

41. Adams, P.D., Afonine, P.V., Bunkóczi, G., Chen, V.B., Davis, I.W., Echols, N., Headd, J.J., Hung, L.W., Kapral, G.J., Grosse-Kunstleve, R.W., et al. (2010). PHENIX: a comprehensive Python-based system for macromolecular structure solution. Acta Crystallogr. D Biol. Crystallogr. *66*, 213–221. https://doi.org/10.1107/S0907444909052925.

42. Blanc, E., Roversi, P., Vonrhein, C., Flensburg, C., Lea, S.M., and Bricogne, G. (2004). Refinement of severely incomplete structures with maximum likelihood in BUSTER-TNT. Acta Crystallogr. D Biol. Crystallogr. *60*, 2210–2221. https://doi.org/10.1107/S0907444904016427.

43. Panjkovich, A., and Svergun, D.I. (2018). CHROMIXS: automatic and interactive analysis of chromatography-coupled small-angle X-ray scattering data. Bioinformatics *34*, 1944–1946. https://doi.org/10.1093/BIOINFORMATICS/BTX846.

44. Manalastas-Cantos, K., Konarev, P.V., Hajizadeh, N.R., Kikhney, A.G., Petoukhov, M.V., Molodenskiy, D.S., Panjkovich, A., Mertens, H.D.T., Gruzinov, A., Borges, C., et al. (2021). ATSAS 3.0: expanded functionality and new tools for small-angle scattering data analysis *54*, 343–355. https://doi.org/10.1107/S1600576720013412.

45. Svergun, D.I. (1999). Restoring Low Resolution Structure of Biological Macromolecules from Solution Scattering Using Simulated Annealing. Biophys. J. *76*, 2879–2886. https://doi.org/10.1016/S0006-3495(99)77443-6.

46. Svergun, D.I., and IUCr. (1992). Determination of the Regularization Parameter in Indirect-Transform Methods Using Perceptual Criteria. J. Appl. Cryst. *25*, 495–503. https://doi.org/10.1107/S0021889892001663.

47. Svergun, D., Barberato, C., Koch, M.H.J., and IUCr. (1995). *CRYSOL* – a Program to Evaluate X-ray Solution Scattering of Biological Macromolecules from Atomic Coordinates. J. Appl. Crystallogr. *28*, 768–773. https://doi.org/10.1107/S0021889895007047.

48. Barozet, A., Molloy, K., Vaisset, M., Zanon, C., Fauret, P., Siméon, T., and Cortés, J. (2022). MoMA-LoopSampler: a web server to exhaustively sample protein loop conformations. Bioinformatics *38*, 552–553. https://doi.org/10.1093/BIOINFORMATICS/BTAB584.

49. Romero-Tamayo, S., Laplaza, R., Velazquez-Campoy, A., Villanueva, R., Medina, M., and Ferreira, P. (2021). W196 and the β -Hairpin Motif Modulate the Redox Switch of Conformation and the Biomolecular Interaction Network of the Apoptosis-Inducing Factor. Oxid. Med. Cell. Longev. *2021*, 6673661. https://doi.org/10.1155/2021/6673661.

50. Salscheider, S.L., Gerlich, S., Cabrera-Orefice, A., Peker, E., Rothemann, R.A., Murschall, L.M., Finger, Y., Szczepanowska, K., Ahmadi, Z.A., Guerrero-Castillo, S., et al. (2022). AIFM1 is a component of the mitochondrial disulfide relay that drives complex I assembly through efficient import of NDUFS5. EMBO J. *41*, e110784. https://doi.org/10.15252/EMBJ.2022110784.

51. Qiu, Y., Wang, H., Fan, M., Pan, H., Guan, J., Jiang, Y., Jia, Z., Wu, K., Zhou, H., Zhuang, Q., et al. (2023). Impaired AIF-CHCHD4 interaction and mitochondrial calcium overload contribute to auditory neuropathy spectrum disorder in patient-iPSC-derived neurons with AIFM1 variant. Cell Death Dis. *14*, 375–414. https://doi.org/10.1038/s41419-023-05899-6.

52. Agirre, J., Atanasova, M., Bagdonas, H., Ballard, C.B., Baslé, A., Beilsten-Edmands, J., Borges, R.J., Brown, D.G., Burgos-Mármol, J.J., Berrisford, J.M., et al. (2023). The CCP4 Suite: Integrative Software for Macromolecular Crystallography. Acta Crystallogr. D Struct. Biol. *79*, 449–461. https://doi.org/10.1107/S2059798323003595.

53. Vagin, A., and Teplyakov, A. (1997). MOLREP: An Automated Program for Molecular Replacement. Acta Crystallogr. D Biol. Crystallogr. *30*, 1022–1025. https://doi.org/10.1107/S0021889897006766.

54. Steiner, R.A., Lebedev, A.A., and Murshudov, G.N. (2003). Fisher's information in maximum-likelihood macromolecular crystallographic refinement. Acta Crystallogr. D Struct. Biol. *59*, 2114–2124. https://doi.org/10.1107/S0907444903018675.

55. Rimoldi, I., Bucci, R., Feni, L., Santagostini, L., Facchetti, G., and Pellegrino, S. (2021). Exploring the copper binding ability of Mets7 hCtr-1 protein domain and His7 derivative: An insight in Michael addition catalysis. J. Pept. Sci. *27*, e3289. https://doi.org/10.1002/PSC.3289.

56. Aliverti, A., Curti, B., and Vanoni, M.A. (1999). Identifying and quantitating FAD and FMN in simple and in iron-sulfur-containing flavoproteins. Methods Mol. Biol. *131*, 9–23. https://doi.org/10.1385/1-59259-266-X:9/COVER.

57. Forneris, F., Orru, R., Bonivento, D., Chiarelli, L.R., and Mattevi, A. (2009). ThermoFAD, a Thermofluor®-adapted flavin ad hoc detection system for protein folding and ligand binding. FEBS J. *276*, 2833–2840. https://doi.org/10.1111/J.1742-4658.2009.07006.X.

58. Pastori, V., Sangalli, E., Coccetti, P., Pozzi, C., Nonnis, S., Tedeschi, G., and Fusi, P. (2010). CK2 and GSK3 phosphorylation on S29 controls wild-type ATXN3 nuclear uptake. Biochim. Biophys. Acta *1802*, 583–592. https://doi.org/10.1016/J.BBADIS.2010.03.007.

59. Yllmaz, Ş., Busch, F., Nagaraj, N., and Cox, J. (2022). Accurate and Automated High-Coverage Identification of Chemically Cross-Linked Peptides with MaxLynx. Anal. Chem. *94*, 1608–1617. https://doi.org/10.1021/ACS.ANALCHEM.1C03688/ASSET/IMAGES/LARGE/AC1C03688_0007.JPEG.

60. Jumper, J., Evans, R., Pritzel, A., Green, T., Figurnov, M., Ronneberger, O., Tunyasuvunakool, K., Bates, R., Žídek, A., Potapenko, A., et al. (2021). Highly accurate protein structure prediction with AlphaFold. Nature *596*, 583–589. https://doi.org/10.1038/s41586-021-03819-2.

61. Winn, M.D., Isupov, M.N., and Murshudov, G.N. (2001). Use of TLS parameters to model anisotropic displacements in macromolecular refinement. Acta Crystallogr. D Biol. Crystallogr. *57*, 122–133. https://doi.org/10.1107/S0907444900014736.

Please cite this article in press as: Fagnani et al., CHCHD4 binding affects the active site of apoptosis inducing factor (AIF): Structural determinants for allosteric regulation, Structure (2024), https://doi.org/10.1016/j.str.2024.02.008

STAR★METHODS

KEY RESOURCES TABLE

REAGENT or RESOURCE	SOURCE	IDENTIFIER
Chemical peptides and recombinant proteins		
CHCHD4 N-terminal peptide	This study	N/A
pKK-AIFΔ101	Churbanova and Sevrioukova[13]	N/A
mutAIF	This study	N/A
Murine CHCHD4	This study	N/A
Oligonucleotides		
accgGTTTTTGCAAAAGCAACTG	This study	N/A
ttatcGGGCAAACTACTATCCAC	This study	N/A
Deposited data		
Structure of oxidized AIF/NAD^+ /N-pep complex	This study	PDB: 8QNS
Software and algorithms		
AlphaFold	Jumper et al.[60]	https://alphafold.ebi.ac.uk/
autoPROC	Vonrhein et al.[36]	https://www.globalphasing.com
CCP4i	Agirre et al.[52]	https://www.ccp4.ac.uk
Molrep	Vagin et al.[53]	https://www.ccp4.ac.uk
Refmac5	Steiner et al.[54]	https://www.ccp4.ac.uk
Buster	Blanch et al.[42]	https://www.globalphasing.com
Phenix	Adams et al.[41]	https://phenix-online.org/
Coot	Emsley et al.[38]	https://www2.mrc-lmb.cam.ac.uk/personal/pemsley/coot/
PyMOL	Schrodinger	https://pymol.org/
ATSAS	Manalastas-Cantos et al.[44]	https://www.embl-hamburg.de/biosaxs/software.html
CHROMIXS	Panjkovich et al.[43]	https://www.embl-hamburg.de/biosaxs/software.htm
Primus	Manalastas-Cantos et al.[44]	https://www.embl-hamburg.de/biosaxs/software.html
Gnome	Svergun[46]	https://www.embl-hamburg.de/biosaxs/software.html
dammin	Svergun[45]	https://www.embl-hamburg.de/biosaxs/software.html
crysol[47]	Svergun et al.[47]	https://www.embl-hamburg.de/biosaxs/software.html
Loop sampler	Barozet et al.[48]	https://moma.laas.fr/

RESOURCE AVAILABILITY

Lead contact

Further information and requests for resources and reagents should be directed to and will be fulfilled by Mario Milani (mario.milani@cnr.it).

Materials availability

All plasmids used in this study will be made available upon request. The study did not generate other new or unique reagents.

Data and code availability

- All data supporting the findings of this study are found within the paper and its Supplementary Information.X-ray structure factor and model have been deposited into the Protein Data Bank under accession number 8QNS.
- This paper does not report original code.
- Any additional information required to reanalyze the data reported in this paper is available from the lead contact upon request.

Please cite this article in press as: Fagnani et al., CHCHD4 binding affects the active site of apoptosis inducing factor (AIF): Structural determinants for allosteric regulation, Structure (2024), https://doi.org/10.1016/j.str.2024.02.008

EXPERIMENTAL MODEL AND STUDY PARTICIPANT DETAILS

The following strains were used in this study.

- Bacterial strain: E. coli strain BL21(DE3); *E. coli* SHuffle® T7.

METHOD DETAILS

Synthesis of CHCHD4 N-terminal peptide (N-pep)

The peptide corresponding to the first 27 N-terminal residues of mouse CHCHD4 (sequence: MSYCRQEGKDRIIFVTKEDHETPSSAE; N-pep) was synthesized by microwave-assisted automated Fmoc/tBu-based solid phase peptide synthesis (MW-SPPS) using a CEM Liberty Blue peptide synthesizer. MW-SPPS was performed on Rink-amide resin (0.4 loading, 0.1 mmol scale) following a standard protocol.[55] All amino acids were N-terminally fluorenylmethoxycarbonyl (Fmoc)-protected and used in a final concentration of 0.2 M in dimethylformamide (DMF). DIC and Oxyma were used as coupling reagents (0.1 M in DMF), and 20% piperidine in DMF for the deprotection. Couplings were performed at 75°C, 170 W for 15 s and then at 90°C, 40 W for 110 s, while deprotection at 75°C, 155 W for 15 s and then at 90°C, 50 W for 50 s. The cocktail cleavage was the following: trifluoroacetic acid/thioanisole/3,6-dioxa-1,8-octanedithiol (92:5:3) for 180 min. After cleavage, the peptide was precipitated from ice-cold diethyl ether and purified by RP-HPLC using an ADAMAS C-18 column from Sepachrom (10 μm, 250 × 21.2 mm) and a gradient elution of 15−60% solvent B (solvent A: water/trifluoroacetic acid 100:0.1; solvent B: acetonitrile/trifluoroacetic acid 100:0.1) over 40 min at a flow rate of 20 ml/min (Figure S9).

AIF and CHCHD4 production

Murine AIF - The pKK233-3 vector-based construct for the bacterial expression of mouse AIF Δ1–101 (from amino acid Gly102; Uniprot: Q9Z0X1) fused with a C-terminal His-tag, named pKK-AIFΔ101 was described previously.[13] AIF was overproduced in *E. coli* strain BL21(DE3) and purified according to the protocol previously reported[13,15] using an ÄKTA-FPLC system (Cytiva). Briefly, after cells sonication, the supernatant fraction was loaded on a Ni^{2+} -affinity column equilibrated in solvent A (50 mM Na-phosphate, pH 8.0, 10 mM imidazole). After extensive washing, AIF was eluted with solvent B (50 mM Na-phosphate, pH 8.0, 500 mM imidazole). As a final purification step, an anion exchange chromatography on a HiLoad 16/10 Q Sepharose HP column, equilibrated in 50 mM Tris-HCl, pH 8.0, 10% glycerol, was performed and protein was eluted using 50 mM Tris-HCl, pH 8.0, 1 M NaCl, 10% glycerol buffer. Purified protein was conserved under anaerobic conditions in N_2-saturated 50 mM Tris-HCl, pH 7.4 (at 25°C), containing 10% glycerol, at -20°C.

The AIF variant harboring the three adjacent amino acyl replacements T503D, V504K and G505P (mutAIF) was obtained by oligonucleotide-directed mutagenesis using the Q5® Site-Directed Mutagenesis Kit (New England BioLabs) and pKK-AIFΔ101 as template. Primers were designed with the NEBaseChanger (New England BioLabs) primer design tool:

For: accgGTTTTTGCAAAAGCAACTG.

Rev: ttatcGGGCAAACTACTATCCAC.

The mutAIF variant was expressed and purified using the same protocol reported for wild type AIF. Both protein forms were stored at -20°C in 50 mM Tris-HCl, pH 7.4 (at 25°C), containing 10% glycerol, and their concentration determined using the extinction coefficient at 452 nm (ε_{452} = 12.54 mM^{-1} cm^{-1}) (see below).

Murine CHCHD4 - A plasmid construct for the bacterial expression of mouse CHCHD4 carrying a thrombin recognition sequence followed by a His-tag at the C-terminus, based on a modified pET-21a(+) vector (Novagen), was purchased from Eurofins Genomics. The protein expression was induced in the *E. coli* SHuffle® T7 strain at mid log phase with 0.2 mM IPTG at 20°C for about 16 h. After cell sonication, the recombinant protein was isolated from the crude cell extract by metal-chelate affinity chromatography using a HisTrap HP cartridge (Cytiva) connected to a ÄKTA-FPLC system (GE Healthcare) and equilibrated in solvent A (50 mM Tris-HCl, pH 8.0, 200 mM NaCl, 10 mM imidazole, 10% glycerol). Protein was eluted using solvent B (50 mM Tris-HCl, pH 8.0, 200 mM NaCl, 500 mM imidazole, 10% glycerol). Final polishing was obtained by anion exchange chromatography on a HiLoad 16/10 Q Sepharose HP column. CHCHD4 was loaded using solvent A (50 mM Tris-HCl, pH 8.0, 10% glycerol) and eluted using solvent B (50 mM Tris-HCl, pH 8.0, 1 M NaCl, 10% glycerol). When needed for specific experiments, after the first purification step the C-terminal tag was cleaved by digestion with thrombin (5 U per milligram substrate protein) for 1 h at 25°C in 50 mM Tris-HCl, pH 8.0, 5 mM $CaCl_2$ and 100 mM NaCl. Possible residual undigested protein was removed by passing the incubation mixture through a HisTrap HP cartridge (Cytiva) prior to the anion exchange step. Purified CHCHD4 was stored at -20°C under anaerobic conditions in N_2-saturated 50 mM Tris-HCl, pH 7.4 (at 25°C), containing 10% glycerol, to prevent sulfhydryl groups oxidation and its concentration determined spectrophotometrically using its extinction coefficient at 280 nm (ε_{280} = 13.310 mM^{-1} cm^{-1}) (see below).

Spectrophotometric analysis

All spectrophotometric measurements were performed using a diode-array 8453 instrument (Agilent). The extinction coefficient of AIF was assessed quantifying the amount of the FAD cofactor released upon protein denaturation induced by the addition of 0.2% SDS.[56] Extinction coefficient and molecular weight of CHCHD4 and the synthetic 27mer peptide corresponding to its N-terminal region were computed using the *ProtParam* software (https://web.expasy.org/protparam/).

Please cite this article in press as: Fagnani et al., CHCHD4 binding affects the active site of apoptosis inducing factor (AIF): Structural determinants for allosteric regulation, Structure (2024), https://doi.org/10.1016/j.str.2024.02.008

The perturbation of the AIF-bound FAD absorption spectrum in the visible region induced by CHCHD4 binding was determined in 50 mM Tris-HCl, pH 8.0, at 25°C. The spectrum of 12.1 μM AIF was recorded before and after the addition of 25.4 μM CHCHD4. To evaluate the possible allosteric effect of CHCHD4 interaction on the binding of NAD^+ to AIF, the spectra of either AIF and an AIF/CHCHD4 mixture were recorded before and after the addition of ca. 4 mM NAD^+. Difference spectra induced by the presence of each ligand were computed by subtracting the appropriate spectrum from that recorded after ligand addition, considering sample dilution.

The effect of the temperature on the affinity of AIF for N-pep was evaluated by recording the spectra of a solution of 12.1 μM, 139 μM, 6.24 mM NAD^+, in 50 mM Tris-HCl, pH 8.0 (at 25°C) over a 4-30°C temperature range. To exclude possible artifacts due to a change in pH induced by the temperature shift, the spectrum of a control solution with the same composition was determined at 25°C before and after the addition of an amount of NaOH able to determine the same increase in pH induced by a 20°C decrease in temperature of the Tris-HCl buffer system. A further control experiment in which CHCHD4 was omitted was performed to verify if NAD^+ could induce any spectral changes on AIF at low temperature.

Thermal unfolding studies

Thermal denaturation of the AIF forms was monitored by the ThermoFAD method, following the changes in FAD fluorescence induced by protein unfolding[57] on 12.1 μM solutions of either proteins in 50 mM Tris-HCl, pH 7.4 (at 25°C), containing 10% glycerol, using a StepOne™ real-time PCR system (Applied Biosystems). When present, NADH and NAD^+ were 1.3 and 6.6 mM, respectively, while CHCHD4 was 15.5 μM. All samples were incubated for 1 h on ice before analysis. A control experiment in which NAD^+ was replaced by a double concentration of phosphate was set to verify if this anion could mimic the dinucleotide.

Analytical Size-exclusion chromatography (SEC)

SEC analyses were performed on 100 μl samples using a Superdex 200 increase 10/30 gel filtration column (GE Healthcare; molecular range: 10 - 600 kDa), with 50 mM Tris-HCl, pH 8.0, 200 mM NaCl, 2 mM DTT, as the mobile phase. Solutions of 20-40 μM AIF forms were incubated for 1 h on ice in the absence and in the presence of 50 μM of CHCHD4 and 2 mM NADH. All separations were performed at 8°C with a flow rate of 0.5 ml/min. SEC experiments on CHCHD4 with/without 5 mM DTT (using a Superdex 75 HR 10/30) did not show any change of the elution profiles.

MicroScale Thermophoresis (MST)

Experiments were performed using either a Monolith NT.155 or a Monolith X apparatus (NanoTemper Technologies GmbH, Munich, Germany) and analyzed with the MO.Affinity Analysis software (NanoTemper Technologies GmbH). His-tagged AIF forms were labeled with the red fluorescent dye NT-647, using the Monolith NT His-Tag Labeling Kit RAD-tris-NTA (NanoTemper Technologies) according to manufacturer instructions. AIF forms, diluted to 200 nM in 1×PBS-T (100 μl), were incubated 1 h on ice either in the absence and in the presence of 500 μM NADH. Each protein sample was mixed with 100 μl of dye solution diluted 1:50 in 1× PBS-T. After 30 min incubation at room temperature, the mixtures were clarified by centrifugation at 15,000 ×g for 10 min at 4°C.

MST measurements were performed at the baseline temperature of 24 °C at a fixed concentration of 50 nM AIF. Titrant CHCHD4 and N-pep concentrations were varied from 4 nM to 140 μM, and from 10 nM to 300 μM, respectively. Laser excitation power and MST power were set to 20% and 40%, respectively.

To unambiguously distinguish between fluorescence changes caused by AIF-CHCHD4 interaction and those caused by non-specific effects, EDTA and EPC tests were performed, according to manufacturer recommendations. The EDTA test was used to exclude possible effects by ligand-induced aggregation or adsorption to capillaries. The EPC test was intended to exclude possible non-specific effects caused by the interaction of the titrant with the His-tag-bound tris-NTA dye. In the first control test, the initial fluorescence of the labeled protein sample was measured before and after EDTA incubation; in the second, the possible effect of CHCHD4 incubation on the MST signal was evaluated on His_6-tagged peptide.

Cross-linking

AIF or mutAIF (27 μM), and CHCHD4 (40 μM) were incubated in 100 mM Na-phosphate, pH 8.0, 150 mM NaCl, 5 mM DTT and 2 mM bis(sulfosuccinimidyl) suberate (BS3), at room temperature. The cross-linking reaction was terminated by the addition of 40 mM Tris-HCl, pH 7.5, after 5, 15, 30 minutes and 1 h, and the samples analyzed by SDS-PAGE. Control experiments were performed using AIF and CHCHD4 alone with/without BS3, and the mixture AIF:CHCHD4 without the cross-linker.

Mass spectroscopy

Each gel band was excised, reduced, alkylated, and digested overnight with trypsin (sequence grade, Sigma-Aldrich) at 37°C using a protease:protein ratio (1:10). Tryptic digests were extracted with 50% ACN in 0.1% TFA, desalted/concentrated on a μZipTipC18 (Millipore) using 50% ACN in 0.1% formic acid as eluent, concentrated using Savant Speed Vac (Thermo Fisher Scientific, Bremen, Germany) and submitted to mass spectrometry.[58] NanoHPLC coupled to MS/MS analysis was performed on Dionex Ultimate 3000 HPLC system with an EASY-SprayTM 2 μm 15 cm × 150 μm capillary column filled with 2 μm C18 100 Å particles, connected to a Q-Exactive Orbitrap (Thermo Fisher Scientific, San Jose, CA, USA). The temperature was set to 35°C and the samples (2 μL) were injected once. MS spectra were collected over an m/z range of 350 – 2000 Da at 70,000 resolutions, operating in the data dependent mode. HCD was performed with collision energy set at 35 eV. Polarity: positive.

The acquired raw files were subjected to data analysis using MaxQuant software (version 2.2.0.0, https://maxquant.org/). The searches were performed against AIF and CHCHD4 sequences. The following settings were applied: BS3 was used as cross-linker, minimum partial score remained as the default value of 10 and minimal score for modified peptides was set at 40. A minimum peptide length of 4 and max peptide mass 6 kDa was used, no contaminants were added, trypsin was set as digestion enzyme with maximum three missed cleavage sites. Carbamidomethylation on cysteine was defined as fixed modification, oxidation of methionine as variable modification.[59]

Alpha fold models

The model of the AIF-CHCHD4 interaction was generated using AlphaFold.[60] More in detail, the ColabFold v1.5.2: AlphaFold2 was used, starting from the amino acid sequences of murine AIF and CHCHD4. The first 5 best poses were analyzed with PyMOL showing high structural similarity. The model of the AIF-CHCHD4 tetrameric assembly was obtained superposing the AlphaFold model of the heterodimer on the crystallographic dimer of the AIF oxidized structure (PDB: 3GD3; with the closed conformation of the C-loop).

Crystallization, data collection and structure refinement

Sitting drop crystallization trials were performed with Oryx-4 crystallization robot (Douglas Instruments), using available commercial crystal screens; the optimal crystallization conditions were selected through several optimization steps starting from the commercial screen JCSG-plus (Molecular Dimensions). AIF and N-pep were mixed with 9 mM NAD^+, to a final concentration of 210 μM and 1 mM, respectively. For every screen condition, 3 droplets were dispensed to a final volume of 0.4 μl with 30%, 50% and 70% of the protein mixture.

The co-crystals were obtained in 20% PEG 6k, 100 mM Tris-HCl pH 8.0 at 4°C. Crystals were cryo-protected in a solution containing 22% PEG 6k, 100 mM Tris-HCl pH 8, 0.6 mM CHCHD4-peptide, and 25% of glycerol, and frozen in liquid nitrogen. Data collection was performed at ESRF (Grenoble) beamline ID30A-1. After indexing and scaling using the autoPROC program[36] (see Table S1 for X-ray data-collection statistics for spherical scaling and Figure S2 for radiation damage during data collection), the crystal structure of reduced AIF (PDB: 3GD4) was used as a model for the molecular replacement.[53] After rigid body refinement,[61] of the 4 AIF molecules in the crystal asymmetric unit (*Refmac5*[54]*;* R/Rfree = 46.6/46.7) followed by restrained refinement (R/Rfree = 32.4/42.4), a residual electron density was clearly visible near the AIF beta strand (aa. 503-507, Figure S3A). After new refinement cycles using global NCS restraints (*Refmac5*; R/Rfree = 31.2/38.6), the mentioned residual electron density was modeled (in one AIF subunit) with a portion of the N-pep, starting from the AlphaFold model of the complex (R/Rfree = 26.5/35.9 after *Refmac5*); afterwards the CHCHD4 peptide was also modeled for the remaining 3 AIF subunits in the crystal a.u. (R/Rfree = 26.3/34.9).

Small-Angle X-ray Scattering (SAXS)

All experiments were performed at the Deutsches Elektronen-Synchrotron (DESY) of Hamburg, Germany, wavelength 0.123985 nm; Detector: Pilatus 6M. CHCHD4 conservation buffer, 50 mM TRIS-HCl, pH 8.0, 200 mM NaCl, 2 mM DTT and for SEC-SAXS, a Superdex 75 10/300 GL column (GE Healthcare) was used. SEC-SAXS data analysis were performed with CHROMIXS and with PRIMUS software of ATSAS suite.

QUANTIFICATION AND STATISTICAL ANALYSIS

Statistical analyses related to the X-ray crystal structures are provided in Table 1. Statistics for SAXS data collection and processing are summarized in Table S3.